Simulation of photoreactive transients and of photochemical transformation of organic pollutants in sunlit boreal lakes across 14 degrees of latitude

Simulation of photoreactive transients and of photochemical transformation of organic pollutants in sunlit boreal lakes across 14 degrees of latitude

Birgit Koehler[a], Francesco Barsotti[b], Marco Minella[b], Tomas Landelius[c], Claudio Minero[b], Lars J. Tranvik[a], Davide Vione[b,*]

[a] Department of Ecology and Genetics/Limnology, Evolutionary Biology Centre, Uppsala University, Norbyvägen 18 D, 75236 Uppsala, Sweden

[b] Department of Chemistry, University of Torino, Via Pietro Giuria 5, 10125 Torino, Italy

[c] Swedish Meteorological and Hydrological Institute, Atmospheric Remote Sensing, Folkborgsvägen 1, 60176 Norrköping, Sweden

* Corresponding author. E-mail: *davide.vione@unito.it.* Phone +39-011-6705296 Fax +39-011-6705242

Abstract

Lake water constituents, such as chromophoric dissolved organic matter (CDOM) and nitrate, absorb sunlight which induces an array of photochemical reactions. Although these reactions are a substantial driver of pollutant degradation in lakes they are insufficiently understood, in particular on large scales. Here, we provide for the first time comprehensive photochemical maps covering a large geographic region. Using photochemical kinetics modeling for 1048 lakes across Sweden we simulated the steady-state concentrations of four photoreactive transient species, which are continuously produced and consumed in sunlit lake waters. We then simulated the transient-induced photochemical transformation of organic pollutants, to gain insight into the relevance of the different photoreaction pathways. We

found that boreal lakes were often unfavorable environments for photoreactions mediated by hydroxyl radicals ($^{\bullet}OH$) and carbonate radical anions ($CO_3^{-\bullet}$), while photoreactions mediated by CDOM triplet states (^{3}CDOM*) and, to a lesser extent, singlet oxygen ($^1O_2$) were the most prevalent. These conditions promote the photodegradation of phenols, which are used as plastic, medical drug and herbicide precursors. When CDOM concentrations increase, as is currently commonly the case in boreal areas such as Sweden, ^{3}CDOM* will also increase, promoting its importance in photochemical pathways even more.

Keywords: Boreal lakes; Browning; Modelling; Photochemistry; Photochemical transients; Pollutants.

1. Introduction

Photochemically induced processes are important for the attenuation of xenobiotics, such as residues of medical drugs and pesticides, in sunlit waters (Fenner et al., 2013). Environmental persistence, defined as the transformation half-life of a chemical, regulates the exposure of organisms to the substance, the extent of its transport and diffuse pollution, and the resilience towards environmental contamination (Boethling et al., 2009; Zou et al., 2015a). To protect resources such as plants, aquatic biota and drinking water, it is therefore crucial to understand the environmental fate and degradation pathways of pollutants (Fenner et al., 2013; Parker et al., 2016). However, little to nothing is known about the role of different photoreactions for pollutant degradation on large geographic scales, especially in boreal regions where the largest lake area on earth is located (Verpoorter et al., 2014). To gain first insight into the relevance of the different photoreaction pathways in boreal lakes we conducted a modeling study, which allowed a large-scale simulation of the likely photochemical behaviour for a range of different compounds. While subject

to a number of necessary assumptions and uncertainties our model simulations contribute, along with laboratory and field measurements which provide more detailed direct observations for specific compounds but are more time- and cost-intensive, a key component towards an integrated approach in assessing chemical persistence in aquatic biomes for different climate zones (Zou et al., 2015a/b).

The photodegradation pathways of pollutants can be divided in direct photolysis and indirect photochemistry. In direct photolysis, degradation is triggered by photon absorption by the pollutant itself. In indirect photochemistry, transformation is caused by reaction with photogenerated transient species (Boreen et al., 2003). These transient species, such as triplet states (^{3}CDOM*), singlet oxygen ($^1O_2$) and hydroxyl radicals ($^{\bullet}$OH), are mostly produced in reactions with photochemical sensitizers such as chromophoric DOM (CDOM) and nitrate (Canonica et al., 2005; Cawley et al., 2015). In the presence of bicarbonate and carbonate, the carbonate radical ($CO_3^{-\bullet}$) is also produced (Canonica et al., 2005). Upon photon absorption, CDOM yields ^{3}CDOM*, $^1O_2$ and $^{\bullet}$OH, while DOM is a sink of $^{\bullet}$OH and $CO_3^{-\bullet}$ (Rosario-Ortiz and Canonica, 2016). Nitrate acts as photochemical $^{\bullet}$OH source and, indirectly, as $CO_3^{-\bullet}$ source in the presence of inorganic carbon via photogenerated $^{\bullet}$OH (Wallace et al., 2010).

Here, we used a unique large-scale dataset of concentration data on total organic carbon (TOC, a measure of DOM) and nitrate as well as inorganic carbon levels, pH values and lake water CDOM absorption spectra, which are available across 14 degrees of latitude for 1048 boreal lakes in Sweden (Koehler et al., 2014). With their comparatively high TOC concentrations, these water environments are representative of boreal lakes in general (Sobek et al., 2007). We combined the observations with atmospheric radiative transfer and aquatic photochemical kinetics modeling, to resolve which photoreaction pathways are generally the most important in boreal lakes, how these reflect in the environmental persistence of chemical compound classes, and how the relevance of photoreaction pathways may change when browning (Larsen et al., 2011) and eutrophication occur.

2. Methods

2.1. Radiation absorption calculations

Water chemical and CDOM absorbance data from 1048 lakes, distributed across Sweden between latitudes from 55°N to 69°N, were obtained from the 2009 Swedish National Lake Inventory which was conducted by the Swedish University of Agricultural Sciences. Lake water had been sampled between 6 September and 24 November 2009, in most cases in the middle of the lake at 0.5 m depth. More details and lake properties have been published earlier (Erlandsson et al., 2012; Koehler et al., 2014).

CDOM-absorbed photons ($P_a^{CDOM,Day}$; mol photons m^{-3} day^{-1}) were calculated for Sep 22, 2009 (autumnal equinox) and 280 to 600 nm (1-nm resolution) from the surface of each lake in 0.005-m-increments down to the target lake depths, as:

$$P_a^{CDOM,Day}(z) = \int_{\lambda_{\min}}^{\lambda_{\max}} E_{od}^{Day}(\lambda,-0)\, a_g(\lambda)\, e^{-(K_d(\lambda)\, z)}\, d\lambda \qquad \text{(eq. 1)}$$

where z is depth (m), λ_{min} and λ_{max} is the minimal and maximal wavelength (nm), $E_{od}^{Day}(\lambda,-0)$ is daily-integrated-downwelling scalar irradiation just below the water surface (mol photons m^{-2} day^{-1} nm^{-1}), a_g is the CDOM Napierian absorption coefficient (m^{-1}) and K_d is the vertical attenuation coefficient for downward irradiance (m^{-1}). The parameter a_g was calculated from measured CDOM absorbance (Koehler et al., 2014). K_d was estimated using regression relationships, with a_g derived from literature data (n=565) for nine wavelengths between 300 and 400 nm. Subsequent fitting of an exponential function was carried out to obtain continuous spectra (Koehler et al., 2014). For each lake, daily-integrated downwelling irradiation just below the water surface ($E_{od}^{Day}(\lambda,-0)$; mol photons m^{-2} day^{-1} nm^{-1}) was simulated for the autumnal equinox 2009 (Sep 22), as described in

detail earlier (Koehler et al., 2014). Briefly, clear-sky downwelling spectra of global and diffuse irradiance reaching the water-air interface were derived for 280 to 600 nm with an hourly time step using the atmospheric radiative transfer model libRadtran 1.6 (Mayer et al., 2011). The clear-sky irradiance spectra were corrected for attenuation by clouds using a cloud effect function (Kasten et al., 1980) which was parameterized using UV irradiance measurements from Norrköping, Sweden, during 2008 (n=2400). Total cloud cover data was retrieved from the archive of the operational mesoscale analysis system MESAN at the Swedish Meteorological and Hydrological Institute (Häggmark et al., 2000). Transmittance of the above water surface irradiance across the air-water interface was calculated separately for the diffuse and direct fraction. The just below water surface hourly diffuse and direct irradiance spectra were converted to downwelling irradiance spectra and integrated to obtain daily irradiation spectra.

Nitrate-absorbed photons ($P_a^{CDOM,Day}$; mol photons m^{-3} day^{-1}) were calculated as:

$$P_a^{NO_3^-,Day}(z) = \int_{\lambda_{min}}^{\lambda_{max}} \frac{\varepsilon_{NO_3^-}(\lambda)\, C_{NO_3^-}}{a_g(\lambda)}\, E_{od}^{Day}(\lambda,-0)\, a_g(\lambda)\, e^{-(K_d(\lambda)\, z)}\, d\lambda \qquad \text{(eq. 2)}$$

where $\varepsilon_{NO_3^-}$ is the molar absorption coefficient of nitrate (L µg N^{-1} m^{-1}) and $c_{NO_3^-}$ is nitrate concentration (µg N L^{-1}). The depth-specific CDOM- and nitrate-absorbed photons were integrated down to z = 0.05 m and down to the average depth (z_{avg}) of each lake using the trapezoid rule. Photon absorption by nitrite was not considered because its concentration was usually below the detection limit of the analytical method and, more importantly, because CDOM usually strongly prevailed over nitrate as $^{\bullet}$OH source. Therefore, it is expected that CDOM out-competes also nitrite for $^{\bullet}$OH generation.

2.2. Photochemical modeling

To calculate the steady-state concentration of the photoreactive transient species, the photon fluxes absorbed by CDOM and nitrate were expressed as $P_a^i(z)$ (where i = CDOM or NO_3^-; mol photons L^{-1} s^{-1}). The formation rates of hydroxyl radicals ($^{\bullet}OH$) and singlet oxygen ($^1O_2$; mol L^{-1} s^{-1}) were calculated as:

$$R_{^{\bullet}OH}^{tot}(z) = R_{^{\bullet}OH}^{CDOM}(z) + R_{^{\bullet}OH}^{NO_3^-}(z) = \Phi_{^{\bullet}OH}^{CDOM} \; P_a^{CDOM}(z) + \Phi_{^{\bullet}OH}^{NO_3^-} \; P_a^{NO_3^-}(z) \qquad \text{(eq. 3)}$$

$$R_{^1O_2}^{tot}(z) = \Phi_{^1O_2}^{CDOM} \; P_a^{CDOM}(z) \qquad \text{(eq. 4)}$$

As the formation quantum yield of $^{\bullet}OH$ by CDOM, $\Phi_{^{\bullet}OH}^{CDOM}$ takes into account all known and poorly known processes of $^{\bullet}OH$ photoproduction by CDOM, including the photo-Fenton reactions triggered by irradiation of Fe species (Vione et al., 2014). The formation quantum yields of photoreactive transients by irradiated CDOM may vary among different aquatic environments, but such variations are more limited than the environmental variability might suggest. Values from available literature sources were used for the relevant quantum yields (Vione et al., 2014).

The steady-state $[^{\bullet}OH]_z$ (mol L^{-1}; day-averaged value referred to a water column of depth z) takes into account the scavenging of $^{\bullet}OH$ by organic matter and inorganic carbon, expressed as:

$$[^{\bullet}OH]_z = \frac{R_{^{\bullet}OH}^{tot}(z)}{k_{OM,^{\bullet}OH} TOC + k_{HCO_3^-,^{\bullet}OH}[HCO_3^-] + k_{CO_3^{2-},^{\bullet}OH}[CO_3^{2-}]} \qquad \text{(eq. 5)}$$

where TOC is total organic carbon (mg_C L^{-1}). The reaction rate constants of $^{\bullet}OH$ with bicarbonate, carbonate and organic matter were derived from the literature (Buxton et al., 1988; Brezonik and Fulkerson-Brekken, 1998).

For $^1O_2$, one should consider its formation by irradiated CDOM ($R_{^1O_2}^{tot}$, eq. 2) and its deactivation upon collision with the water solvent, which has a first-order rate constant of $k_d = 2.5 \cdot 10^5$ s^{-1}. Therefore, the steady-state $^1O_2$ concentration is $[^1O_2]_z = R_{^1O_2}^{tot}(z) \; k_d^{-1}$ (Latch and McNeill, 2006).

The carbonate radical ($CO_3^{-\bullet}$) is produced by $^{\bullet}OH$ oxidation of inorganic carbon (HCO_3^- and CO_3^{2-}) and by ^{3}CDOM* oxidation of CO_3^{2-} (Canonica et al., 2005). The two pathways give the following formation rates for $CO_3^{-\bullet}$ (mol L^{-1} s^{-1}) (Bodrato and Vione, 2014):

$$R_{CO_3^{-\bullet}}^{^{\bullet}OH}(z) = [^{\bullet}OH]_z \ (k_{HCO_3^-,^{\bullet}OH}[HCO_3^-] + k_{CO_3^{2-},^{\bullet}OH}[CO_3^{2-}]) \quad \text{(eq. 6)}$$

$$R_{CO_3^{-\bullet}}^{CDOM}(z) = \eta_{CO_3^{-\bullet}}^{CDOM}\ [CO_3^{2-}]\, P_a^{CDOM}(z) \quad \text{(eq. 7)}$$

It is $R_{CO_3^{-\bullet}}^{tot}(z) = R_{CO_3^{-\bullet}}^{CDOM}(z) + R_{CO_3^{-\bullet}}^{^{\bullet}OH}(z)$ and, usually, $R_{CO_3^{-\bullet}}^{CDOM}(z) < R_{CO_3^{-\bullet}}^{^{\bullet}OH}(z)$. $CO_3^{-\bullet}$ is mostly scavenged by DOM, and its steady-state concentration (mol L^{-1}) was expressed as:

$$[CO_3^{-\bullet}]_z = \frac{R_{CO_3^{-\bullet}}^{tot}(z)}{k_{CO_3^{-\bullet},DOM}\, TOC} \quad \text{(eq. 8)}$$

where $k_{CO_3^{-\bullet},DOM}$ was taken as the average of available literature values (Canonica et al., 2005).

Finally, the CDOM triplet states (^{3}CDOM*) are produced by CDOM irradiation and are deactivated by a number of processes, including internal conversion and reaction with dissolved O_2. These processes can be described by an overall first-order rate constant $k' \cong 5 \cdot 10^5$ s^{-1} (Canonica and Freiburghaus, 2001). The steady-state $[^3CDOM^*]_z$ (mol L^{-1}) was expressed as:

$$[^3CDOM^*]_z = \frac{\Phi_{^3CDOM^*}^{CDOM}\, P_a^{CDOM}(z)}{k'} \quad \text{(eq. 9)}$$

with $\Phi_{^3CDOM^*}^{CDOM}$ taken from the literature (Vione et al., 2014).

2.3. Kinetics of direct and indirect pollutant photolysis

A rather simple way to assess the environmental significance of the transient steady-state concentrations calculated previously is to see how they may translate into the degradation kinetics of xenobiotics with known photoreactivity. As first model substance we chose the pharmaceutical

acetaminophen which is commonly found in Swedish lakes (Zou et al., 2015a) and reacts with $CO_3^{\bullet-}$ (De Laurentiis et al., 2014). Apart from acetaminophen, however, the xenobiotics that are commonly found in Swedish lakes, such as diclofenac or ibuprofen (Zou et al., 2015a/b), either have poorly known photoreactivity, or do not cover a sufficiently wide range of photochemical reactivity to provide insight into the general photochemical behavior of Swedish lakes. For these reasons, they are hardly suitable to assess the phototransformation pathways of boreal lakes. Therefore, in addition to acetaminophen (APAP), we chose four more model pollutants for which: 1) all or at least the majority of the relevant photochemical reaction rate constants are known (Table 1); 2) the reaction pathways differ strongly, and 3) the photochemical behavior is already known for temperate lakes (Avetta et al., 2014; De Laurentiis et al., 2014; Passananti et al., 2014; Fabbri et al., 2015; Vione et al., 2015). Specifically, we chose the fungicide dimethomorph (DMM), the solar filter ethylhexyl methoxycinnamate (EHMC), the herbicide fenuron (FEN) and nicotine (NIC). We included EHMC because it undergoes very efficient direct photolysis (Vione et al., 2015), as well as DMM and FEN because of the significant role played by ^{3}CDOM*, together with $^\bullet$OH, in their transformation (Avetta et al., 2014; Fabbri et al., 2015). NIC was chosen because it is almost exclusively photodegraded by reaction with $^\bullet$OH (Passananti et al., 2014).

Assume a pollutant substrate S at concentration [S] (mol L^{-1}), which can be degraded by direct photolysis and by reaction with $^\bullet$OH, $CO_3^{-\bullet}$, $^1O_2$ and ^{3}CDOM*. Assume also the following key parameters for S: photolysis quantum yield Φ_S, absorbed photon flux $P_a^S(z)$ (mol photons L^{-1} s^{-1}), and second-order reaction rate constants $k_{S,J}$ (L mol^{-1} s^{-1}), where J = $^\bullet$OH, $CO_3^{-\bullet}$, $^1O_2$ or ^{3}CDOM*.

The degradation rate of S due to photochemical reactions is the following (mol L^{-1} s^{-1}):

$$R_S(z) = \Phi_S \, P_a^S(z) + [S] \sum_J k_{S,J} \, [J]_z \qquad \text{(eq. 10)}$$

where $[J]_z$ (mol L^{-1}) is the daily- and depth-averaged steady-state concentration of the transient species *J* (calculated as described above), referred to the depth *z*. The values of Φ_S and $k_{S,J}$ were parameterized according to Table 1.

$P_a^S(z)$ (mol photons L^{-1} s^{-1}) was calculated as:

$$P_a^S(z) = [S] \int_{\lambda_{\min}}^{\lambda_{\max}} \frac{\varepsilon_S(\lambda)}{a_g(\lambda)} \cdot E_{od}^{Day}(\lambda,-0)\, a_g(\lambda)\, e^{-(K_d(\lambda) z)}\, d\lambda \qquad \text{(eq. 11)}$$

where $\varepsilon_S(\lambda)$ is the molar absorption coefficient of S (L mol^{-1} cm^{-1}). The pseudo-first order degradation rate constant is $k_S(z) = R_S(z)[S]^{-1}$. The value of $k_S(z)$ is independent of [S], provided that the latter is very low (e.g., below 1 μmol L^{-1}) and does not affect $P_a^{CDOM}(z)$. Note that the main light absorber in surface waters is CDOM, with usually negligible contributions from other solution constituents (Loiselle et al., 2008). The rate $R_S(z)$ is expressed in mol L^{-1} s^{-1} units, thus $k_S(z)$ has units of s^{-1}. More intuitive data can be obtained with units of day^{-1}, as $k_S^{Day}(z) = (8.5 \cdot 10^4)^{-1}\, k_S(z)$. The half-life time of S in day units, in a water column of depth *z*, is given by: $t_{1/2}^{Day}(z) = \ln 2\, (k_S^{Day}(z))^{-1}$.

2.4. Model assumptions

First of all, phototransformation kinetics of the model compounds was determined under the assumption of thorough mixing of the lake water. For model parameterization, we assumed that certain photochemical parameters are universally valid because they are referred to substances that do not vary in nature among different environments, and specifically: the formation quantum yield of $^{\bullet}OH$ by nitrate; the reaction rate constants of $^{\bullet}OH$ with bicarbonate and carbonate (Buxton et al., 1988; Vione et al., 2009); the reaction rate constants of APAP, DMM, EHMC, FEN and NIC with $^{\bullet}OH$, $CO_3^{-\bullet}$ and $^1O_2$ (Avetta et al., 2014; De Laurentiis et al., 2014; Passananti et al., 2014; Fabbri

et al., 2015; Vione et al., 2015), as well as the first-order inactivation rate constant of $^1O_2$ upon collision with the water solvent (Latch and McNeill, 2006). However, other photochemical parameters may depend on the environment, such as the formation quantum yields of the transient species from irradiated CDOM, the reaction rate constants of $^{\bullet}OH$ and $CO_3^{-\bullet}$ with DOM, the first-order inactivation rate constant of ^{3}CDOM*, and the second-order reaction rate constants of ^{3}CDOM* with APAP, DMM, EHMC and FEN. These parameters were taken from the literature (Brezonik and Fulkerson-Brekken, 1998; Canonica and Freiburghaus, 2001; Canonica et al., 2005; Vione et al., 2014), but all the cited studies were conducted in temperate water samples. Hence, there is a degree of uncertainty of how appropriate it is to use these values for boreal lakes. We justify this model assumption with the fact that DOM was found to show only a limited modelcular and photochemical variability across inland waters worldwide. Specifically, ultrahigh-resolution mass spectrometry revealed a substantial overlap in molecular-level patterns for DOM in inland waters across biomes and continents (Kellerman et al., 2014). The individual compounds were largely overlapping between fresh DOM prior to substantial light exposure in boreal lakes and photolabile compounds from Congo River water, and *vice versa* (i.e., DOM with substantial light exposure and photoresistant DOM) (Stubbins et al. 2010; Kellerman et al. 2014). Also, the wavelength-integrated apparent quantum yield for photochemical DOM mineralization varied by only a factor of 12 across a variety of boreal, polar, temperate, and tropical lakes, including saline lagoons, which covered a very wide range in chemical and optical water properties (Koehler et al., 2016). Finally, considering that boreal lakes appear to be favourable environments for reactions triggered by ^{3}CDOM* and $^1O_2$ (*vide infra*), the values we used here for $\Phi^{CDOM}_{^3CDOM*}$ and $\Phi^{CDOM}_{^1O_2}$ are in the lower range of those reported for temperate water bodies (Vione et al., 2014). Therefore, we likely underestimated the formation of ^{3}CDOM* and $^1O_2$ in boreal lake water, i.e. we conducted a conservative calculation. All lake photoactivity parameters used in the model are reported in Table SM1 of the Supplementary Material (hereafter SM).

2.5. Model validation

To assess the performance of the atmospheric radiative transfer model under clear-sky conditions, UV irradiance observed during 2008 in Norrköping in Southern Sweden, with a total cloud cover of less than 10%, was compared to clear-sky irradiance simulated for the same place and time. A linear regression between observed and simulated clear-sky irradiance gave a R^2 of 0.998 (n=996). Cloud-corrected irradiance was validated using a 100-fold cross validation in which, for each subvalidation, 2375 observations were used for regression and 25 observations were used for prediction. For overcast sky with total cloud cover exceeding 90% the mean bias error was 1.2% and the normalized root mean squared error was 29% (Koehler et al., 2014). CDOM-absorbed photons calculated similarly as for this study were earlier used to simulate photochemical CDOM mineralization rates in the water column, and proved to be in good agreement with observed depth profiles (Koehler et al., 2014; Groeneveld et al., 2015).

The approach used to calculate the steady-state concentrations of photoreactive transients and the photochemical half-life times of xenobiotics has been previously validated by comparison with available field data of surface-water photoreactivity in European temperate water bodies. The half-life times predicted by the model were usually comparable with field ones, within the respective uncertainties of both model predictions and field assessments, or they were included within the variability range provided for the field data (Bodrato and Vione, 2014).

To validate the pollutant degradation modeling we used observations on the persistence of two xenobiotics in Swedish lakes, specifically for carbamazepine in Norra Bergundasjön and for ibuprofen in Boren (Zou et al., 2015a/b). Validation was possible for these two compounds because their photochemical reactivity is sufficiently known, at least as far as the main photoreaction pathways are concerned, and photochemistry may play an important role in their attenuation (Matamoros et al., 2009). The potential importance of photochemistry in the attenuation of

carbamazepine and ibuprofen is suggested by a comparison between the observed persistence (Zou et al., 2015a/b) and the known biodegradation kinetics (Quintana et al., 2005; Benotti and Brownawell, 2009; Girardi et al., 2013). For the validation simulation for Norra Bergundasjön we used water chemistry data measured during May to October 2015 (H. Olofsson, unpublished data), irradiance spectra simulated for the same place and time period and the lake average depth of 3.3 m. The photochemical kinetics model estimated $[^{\bullet}OH]_{ave} = (1\text{-}2)\cdot10^{-18}$ mol L^{-1}. We then assumed that carbamazepine mainly reacts with $^{\bullet}OH$ (De Laurentiis et al., 2012) and used the reported second-order reaction rate constant of the process ($k_{Carbamazepine,^{\bullet}OH} = 8\cdot10^{9}$ L mol^{-1} s^{-1}; Wols and Hofman-Caris, 2012) to calculate the half-life time. For the validation simulation for Boren we used average water chemistry data from 2013 to 2015 (http://ext-dokument.lansstyrelsen.se/Ostergotland/MSV/sjo/Mo03.pdf), irradiance spectra simulated for the same place and time period and the lake average depth of 5.4 m. Ibuprofen is mainly transformed by $^{\bullet}OH$ and $^{3}CDOM^{*}$ reactions, and in both cases the reaction rate constants are $\sim1\cdot10^{10}$ L mol^{-1} s^{-1} (Vione et al., 2011; Wols and Hofman-Caris, 2012). The photochemical kinetics model estimated $[^{\bullet}OH] = (5\text{-}15)\cdot10^{-18}$ mol L^{-1} and $[^{3}CDOM^{*}] = (7\text{-}20)\cdot10^{-17}$ mol L^{-1}, which allowed us to calculate half-life times.

2.6. Statistical analyses

Principal components analysis (PCA) was carried out on column-autoscaled data using the chemometric software V-Parvus on the whole dataset (1048 samples, 18 variables). The percent explained variance on the first and second principal component was 38.9 and 23.2%, respectively. Loadings analysis emphasises interrelationships among variables where correlations, anti-correlations and non-correlations correspond to parallel, anti-parallel and perpendicular loadings, respectively (Forina et al., 2008). Relationships between the steady-state concentrations of the

simulated photoreactive transients and the concentrations of total organic carbon and nitrate, as well as the irradiance, were analyzed using linear least square regression models. Right-skewed variables were logarithmically transformed before analysis, after adding a small constant value if the dataset included zero values. Model significance was assessed using regression analysis of variance. Differences were considered significant if P value ≤ 0.05. Linear regression lines are shown for the relationships where $R^2>0.25$. Analyses were conducted using R3.1.1 (R.D.C. Team, 2014).

2.7. Data representation

Color-coded maps visualizing patterns across the Swedish lakes were produced using the Sweden *rds* file provided in the Database of Global Administrative Areas (GADM) 2015 (http://gadm.org/country), and the function *spplot* of the R package *sp* in R3.1.1 (R.D.C. Team, 2014).

3. Results and Discussion

3.1 Concentrations and control of photoreactive transient species

The spatial distribution of TOC (Fig. 1a) was mirrored in the simulated steady-state concentrations of CDOM triplet states in the 5-cm upper layer of the water column, $[^3CDOM^*]_{5cm}$ (Fig. 2a). The same was the case for singlet oxygen, $[^1O_2]_{5cm}$ (Fig. SM1a in SM). Coherently, a principal component analysis (PCA) revealed strong correlations of $[^3CDOM^*]_{5cm}$ and $[^1O_2]_{5cm}$ with TOC, as shown by the similar loading values for these variables (Fig. 3). Considering that high-TOC waters are generally rich in CDOM (Loiselle et al., 2008; Rosario-Ortiz and Canonica, 2016), this correlation is simultaneously caused by elevated $^3CDOM^*$ and $^1O_2$ formation rates following photon absorption by CDOM in the water surface layer, and by deactivation of $^3CDOM^*$ and $^1O_2$ that is largely independent of TOC (Latch and McNeill, 2006).

Both the simulated $[^3CDOM^*]_{5cm}$ and the $[^3CDOM^*]_{avg}$ values (the latter referred to the average lake depth avg) were lower in north-western Sweden (Fig. 2a/b), where TOC concentrations are usually low (often <5 $mg_C\ L^{-1}$, Fig. 1a). For $[^3CDOM^*]_{avg}$ the correlation with TOC was weaker compared to $[^3CDOM^*]_{5cm}$ (Fig. 3), likely because the photochemically active photons are largely absorbed by CDOM in the first meter of the water column across the study lakes (absorption saturation) (Koehler et al., 2014). Consequently, photochemistry is inhibited in the poorly illuminated deeper water layers (Wenk et al., 2011; Aarnos et al., 2012), dampening the TOC-$^3CDOM^*$ relationship. Only a small amount in the variability of simulated photoreactive transients was explained by the photon flux (Fig. SM2; $R \leq 0.25$). In the present case (fall equinox in Sweden) irradiance variations across the country were relatively limited and largely linked to the latitude, allowing other factors to play a more important role. Indeed, the photochemical production of transient species depends not only on the irradiance but, most notably, on water chemistry and depth. In some cases ($^3CDOM^*$ and $^1O_2$) the chemistry only influences the photoproduction processes, while in other cases ($^{\bullet}OH$ and $CO_3^{\bullet-}$) it affects both formation and scavenging of the transients (Vione et al., 2014).

In the water column of lakes, the irradiance absorption saturation induces a plateau in the formation rate of $^{\bullet}OH$ with increasing CDOM, but a similar effect does not take place for $^{\bullet}OH$ scavenging by DOM (Vione et al, 2014). Consequently, we found $^{\bullet}OH$ scavenging to be a major factor that controlled the simulated $[^{\bullet}OH]_{avg}$ in the high-TOC lakes under study, producing low $[^{\bullet}OH]_{avg}$ levels compared to temperate lakes (Minella et al., 2016). In our case, the lakes with the highest $[^{\bullet}OH]_{avg}$ values were the relatively low-TOC lakes of north-western Sweden (Fig. 2d). The radical $CO_3^{-\bullet}$ is mainly formed upon oxidation of inorganic carbon by $^{\bullet}OH$. Because DOM scavenges both $CO_3^{-\bullet}$ and $^{\bullet}OH$, involved in $CO_3^{-\bullet}$ generation (Vione et al., 2014), the simulated $[CO_3^{-\bullet}]_{5cm}$ and $[CO_3^{-\bullet}]_{avg}$ values were usually higher in the low-TOC lakes of north-western Sweden than in other parts of the

country (Fig. 2e,f), and low compared to temperate regions (Canonica et al., 2005; Minella et al., 2016).

3.2 Indirect photochemical pollutant degradation

Performance of the pollutant degradation modeling was assessed by comparing simulated vs. observed half-life times of two compounds for two Swedish lakes (Zou et al., 2015a/b). Specifically, a half-life time of 1400 days had been measured for carbamazepine in Norra Bergundasjön in late spring, with a 95% confidence interval of 780-5700 days (Zou et al., 2015a). Our model calculated half-life times of 400-900 days, which is in reasonable agreement with the observations. Moreover, the observed half-life time of ibuprofen was 4-10 days in lake Boren (Zou et al., 2015b). The simulated half-life times of 3.5-10.6 days, mostly due to the reactions with ^{3}CDOM*, were almost exactly in the same range as the field observations. This finding suggests that CDOM in boreal lakes can trigger ^{3}CDOM*-induced triplet sensitisation processes, in agreement with findings concerning the elevated CDOM photoactivity in polar environments (De Laurentiis et al., 2013). Hence, in both validation cases the model predictions derived from the steady-state concentrations of the photoreactive transient species were accurate within a factor of maximally two when compared to field data, which is a reasonable result for the modelling of xenobiotics phototransformation. The successful validation provides confidence that the model predictions can be extended to other pollutants as well. In particular, in order to get insight into the details of the prevailing photochemical processes in Swedish lakes, we chose five compounds that span a wide range of reactivity and allow by photochemical fate modeling for a thorough assessment of the main photoreaction pathways in Swedish lake water. The assessment was carried out by comparing model predictions for boreal lakes with the well-known behavior of the chosen molecules in temperate environments. While our simulation study allowed a first large-scale assessment of the likely photochemical behaviour for a range of compounds in boreal lakes,

laboratory and field studies are needed to provide detailed system- and compound-specific observations and substantiate the patterns we found using photochemical modeling.

The generally high CDOM content in the study lakes restricts sunlight penetration into the water column and hence direct photolysis of pollutants. This makes the simulated photoreactive transient species highly relevant for indirect photochemical degradation (Wallace et al., 2010; Wenk et al., 2011; Rosario-Ortiz and Canonica, 2016). To gain insight into the photoreaction pathways prevailing in boreal lakes, we considered the half-life times of the anthropogenic pollutants APAP, DMM, EHMC, FEN and NIC, referred to the average lake depth. The simulated half-life times ($t_{½}$), which are inversely proportional to the photodegradation rate constants, ranged from weeks for EHMC and APAP to months for DMM and FEN (Fig. 4a-d, Table 2). The median water retention time of 24742 Swedish lakes amounted to 120 days, with a range of 7 days to 3.3 years between the 2.5th and the 97.5th percentiles (Müller et al., 2013). Therefore, with the exception of NIC with many years of photochemical lifetime (see below), the predicted photochemical lifetimes of our model compounds were on the short end of the typical water retention times in Swedish lakes.

The longest $t_{½}$ values of APAP, DMM and FEN were found in the north-western lakes, where the lowest values of $[^3CDOM^*]_{avg}$ were predicted. In agreement, the pseudo first-order photodegradation rate constants of APAP, DMM and FEN correlated positively with $[^3CDOM^*]_{avg}$ (Fig. 3), suggesting that their phototransformation was almost exclusively accounted for by $^3CDOM^*$. This is different from the general behavior in temperate water bodies, where $CO_3^{-\bullet}$ is a key photoreactive transient in the photodegradation of APAP and where $^\bullet OH$ plays important roles in DMM and FEN transformation (Table 2) (Avetta et al., 2014; De Laurentiis et al., 2014; Fabbri et al., 2015). The simulated photochemical half-life times of NIC, which mainly reacts with $^\bullet OH$ (Passananti et al., 2014), reached up to years or even a few decades in high-TOC boreal lakes (Fig. 4e, Table 2), in accordance with the low values of $[^\bullet OH]_{avg}$ in these environments. This finding means that biodegradation (Benotti and Brownawell, 2009) would be by far the main transformation

pathway for NIC in lake water, with a mostly negligible contribution by photochemistry. By comparison, photochemical half-life times of several months are expected for NIC in temperate lakes (Table 2) (Passananti et al., 2014). Overall, the general conditions that prevail in many of the studied Swedish lakes would favour the reactions induced by ^{3}CDOM* to the detriment of processes induced by $^{\bullet}$OH and $CO_3^{-\bullet}$.

3.3 Photochemical behaviour of boreal lakes

The results of the above photochemical modeling can be extended to broader classes of naturally-occurring molecules and anthropogenic pollutants (Table 2). Most notably, indirect photoreactions with ^{3}CDOM* can induce effective degradation of phenols and phenylurea herbicides (Gerecke et al., 2001). Also, ^{3}CDOM* is an important source of the reactive oxygen species $O_2^{-\bullet}$ and of hydrogen peroxide (H_2O_2), through oxidation of organic compounds by electron or hydrogen transfer followed by reaction with oxygen (Richard et al., 2007). These and other species are involved in the decomposition of CDOM and can impose oxidative stress on aquatic organisms (Aarnos et al., 2012; Glaeser et al., 2014). High (C)DOM lakes would also be favorable environments for degradation processes induced by $^1O_2$, which had a similar geographic distribution as ^{3}CDOM* (Fig. SM1). Singlet oxygen is important in the phototransformation of anionic chlorophenols, commonly used as pesticides, herbicides and disinfectants (Gerdes et al., 1997). In low-(C)DOM boreal lakes, $CO_3^{-\bullet}$ could significantly photodegrade aromatic amines and thiols, which are widely used for pesticides, pharmaceuticals, dyes and odors (Larson and Zepp, 1988). Moreover, $^{\bullet}$OH could significantly oxidize refractory pollutants such as the pharmaceutical carbamazepine (Table 1) (Yan and Song, 2014).

The xenobiotics that would accumulate in high-CDOM boreal lakes are biorefractory compounds prevalently reacting with $^{\bullet}$OH or $CO_3^{-\bullet}$. However, due to similar reduction potentials of ^{3}CDOM*

and $CO_3^{-\bullet}$ (Canonica et al., 2005; Rosario-Ortiz and Canonica, 2016), compounds are unlikely to react fast with $CO_3^{-\bullet}$ and be at the same time unreactive toward ^{3}CDOM*. An exception may be represented by some aromatic amines that are oxidized fast by ^{3}CDOM* in a first reaction step, but that undergo efficient back-reduction (and hence inhibition of degradation) in the presence of elevated DOM levels (Wenk et al., 2011). Moreover, accumulation is expected for biorecalcitrant xenobiotics that mainly react with $^{\bullet}$OH, such as for instance carbamazepine (the second most refractory pollutant in lake Norra Bergundasjön, southern Sweden; Zou et al., 2015b) and some hydrocarbons (Table 2).

3.4 Effects of eutrophication and browning

TOC and nitrate levels in a given lake may undergo long-term changes because of phenomena such as increasing CDOM concentration (browning) (Monteith et al., 2007; Larsen et al., 2011) and eutrophication (Quirós, 2003). Using a space-for-time replacement approach, the correlation plots of the simulated steady-state concentrations of the photoreactive transient species with TOC and nitrate give some insight into the possible impact of such increases (Figs. 5 and SM3). Specifically, given that $[^3\text{CDOM*}]_{5\text{cm}}$ (Fig. 5a; R^2=0.76 and P<0.001) and $[^1\text{O}_2]_{5\text{cm}}$ (Fig. SM3a; R^2=0.76 and P<0.001) were positively correlated with TOC, TOC changes will proportionally modify these transient concentrations. The correlation was weaker but still significant for $[^3\text{CDOM*}]_{\text{avg}}$ (Fig. 5b; R^2=0.29 and P<0.001) and $[^1\text{O}_2]_{\text{avg}}$ (Fig. SM3b; R^2=0.29 and P<0.001). For instance, assuming irradiance and water depth do not undergo important variations, a doubling of TOC from 10 to 20 $\text{mg}_\text{C}\ \text{L}^{-1}$ would produce on average a ~60% increase in $[^3\text{CDOM*}]_{\text{avg}}$ and $[^1\text{O}_2]_{\text{avg}}$. In contrast, the inverse relationships between TOC and $[^{\bullet}\text{OH}]_{\text{avg}}$ (R^2=0.33 and P<0.001) and $[\text{CO}_3^{-\bullet}]_{\text{avg}}$ (R^2=0.31 and P<0.001) suggest that $^{\bullet}$OH- and $CO_3^{-\bullet}$-induced reactions would be further inhibited by browning (Fig. 4d,f). Differently from TOC, we found no strong relationships between the

simulated photoreactive transients and nitrate (all $R^2 \leq 0.17$; Fig. SM4). This result is expected for ^{3}CDOM* given that nitrate plays no role in its generation or deactivation. In the case of $^{\bullet}$OH it indicates that CDOM strongly prevailed over nitrate as $^{\bullet}$OH source. Hence, as opposed to TOC changes, nitrate changes brought about by, e.g., eutrophication will not have considerable consequences for indirect photochemical reactions in boreal lakes.

4. Conclusions

Lakes are more numerous at boreal and arctic latitudes than anywhere else on Earth (Verpoorter et al., 2014), and lakes in these areas commonly exhibit high CDOM concentrations. We conclude that ^{3}CDOM*-mediated photoreactions controlled by water chemistry are likely highly important processes behind the transformation of natural and anthropogenic organic compounds in these waters. The conditions in boreal lakes could favour the phototransformation of phenolic compounds including the chlorophenolates, and of phenylureas. With ongoing climate change, DOM and CDOM concentrations are expected to increase in northern inland waters (Larsen et al., 2011), which we expect to further facilitate these ^{3}CDOM*-mediated photoreactions at the expense of direct photolysis and the processes mediated by $^{\bullet}$OH and $CO_3^{-\bullet}$.

Acknowledgements. BK and LT acknowledge funding from the Swedish Research Council for Environment, Agricultural Sciences and Spatial Planning (FORMAS) as part of the research environment "The Color of Water" (grant 2009-1350-15339-81), from the Swedish Research Council (grant 2011-3475-88773-67) and from the Knut and Alice Wallenberg Foundation (grant KAW 2013.0091). DV, MM and CM acknowledge funding from MIUR-PNRA. We are grateful to Håkan Olofsson for water chemistry data from lake Norra Bergundasjön.

References

Aarnos, H., Ylöstalo, P., Vähätalo, A. V., 2012. Seasonal phototransformation of dissolved organic matter to ammonium, dissolved inorganic carbon, and labile substrates supporting bacterial biomass across the Baltic Sea. J. Geophys. Res. 117, G01004.

Avetta, P., Marchetti, G., Minella, M., Pazzi, M., De Laurentiis, E., Maurino, V., Minero, C., Vione, D., 2014. Phototransformation pathways of the fungicide dimethomorph ((E, Z) 4-[3-(4-chlorophenyl)-3-(3, 4-dimethoxyphenyl)-1-oxo-2-propenyl] morpholine), relevant to sunlit surface waters. Sci. Total Environ. 500, 351–360.

Benotti, M. J., Brownawell, B. J., 2009. Microbial degradation of pharmaceuticals in estuarine and coastal seawater. Environ. Pollut. 157, 994-1002.

Bodrato, M., Vione, D., 2014. APEX (Aqueous Photochemistry of Environmentally occurring Xenobiotics): A free software tool to predict the kinetics of photochemical processes in surface waters. Environ. Sci.-Process Impacts 16, 732–740.

Boethling, R., Fenner, K., Howard, P., Klečka, G., Madsen, T., Snape, J. R., Whelan, M. J., 2009. Environmental persistence of organic pollutants: guidance for development and review of POP risk profiles. Integr. Environ. Assess. Manag. 5, 539-556.

Boreen, A. L., Arnold, W. A., McNeill, K., 2003. Photodegradation of pharmaceuticals in the aquatic environment: A review. Aquat. Sci. 65, 320-341.

Brezonik, P. L., Fulkerson-Brekken, J., 1998. Nitrate-induced photolysis in natural waters: Controls on concentrations of hydroxyl radical photo-intermediates by natural scavenging agents. Environ. Sci. Technol. 32, 3004-3010.

Buxton, G. V., Greenstock, C. L., Helman, W. P., Ross, A. B., 1988. Critical review of rate constants for reactions of hydrated electrons, hydrogen atoms and hydroxyl radicals ($^{\bullet}OH/^{\bullet}O^{-}$ in aqueous solution. J. Phys. Chem. Ref. Data 17, 513–886.

Canonica, S., Freiburghaus, M., 2001. Electron-rich phenols for probing the photochemical reactivity of freshwaters. Environ. Sci. Technol. 35, 690-695.

Canonica, S., Kohn, T., Mac, M., Real, F. J., Wirz, J., von Gunten, U., 2005. Photosensitizer method to determine rate constants for the reaction of carbonate radical with organic compounds. Environ. Sci. Technol. 39, 9182–9188.

Cawley, K. M., Korak, J. A., Rosario-Ortiz, F. L., 2015. Quantum yields for the formation of reactive intermediates from dissolved organic matter samples from the Suwannee River. Environ. Eng. Sci. 32, 31–37.

De Laurentiis, E., Chiron, S., Kouras-Hadef, S., Richard, C., Minella, M., Maurino, V., Minero, C., Vione, D., 2012. Photochemical fate of carbamazepine in surface freshwaters: Laboratory measures and modelling. Environ. Sci. Technol. 46, 8164-8173.

De Laurentiis, E., Buoso, S., Maurino, V., Minero, C., Vione, D., 2013b. Optical and photochemical characterization of chromophoric dissolved organic matter from lakes in Terra Nova Bay, Antarctica. Evidence of considerable photoreactivity in an extreme environment. Environ. Sci. Technol. 47, 14089-14098.

De Laurentiis, E., Prasse, C., Ternes, T. A., Minella, M., Maurino, V., Minero, C., Sarakha, M., Brigante, M., Vione, D., 2014. Assessing the photochemical transformation pathways of acetaminophen relevant to surface waters: transformation kinetics, intermediates, and modelling. Water Res. 53, 235–248.

Erlandsson, M., Futter, M. N., Kothawala, D., Koehler, S. J., 2012. Variability in spectral absorbance metrics across boreal lake waters. J. Environ. Monit. 14, 2643–2652.

Fabbri, D., Minella, M., Maurino, V., Minero, C., Vione, D., 2015. Photochemical transformation of phenylurea herbicides in surface waters: A model assessment of persistence, and implications for the possible generation of hazardous intermediates. Chemosphere 119, 601–607.

Fenner, K., Canonica, S., Wackett, L. P., Elsner, M., 2013. Evaluating pesticide degradation in the environment: blind spots and emerging opportunities. Science 341, 752–758.

Forina, M., Lanteri, S., Armanino, C., Oliveros, M. C., Casolino, C., 2008. V-PARVUS. An extendable package of programs for explorative data analysis, classification and regression analysis. Dip. Chimica e Tecnologie Farmaceutiche ed Alimentari, University of Genoa, Italy.

Gerdes, R., Wöhrle, D., Spiller, W., Schneider, G., Schnurpfeil, G., Schulz-Ekloff, G., 1997. Photo-oxidation of phenol and monochlorophenols in oxygen-saturated aqueous solutions by different photosensitizers. J. Photochem. Photobiol. A-Chem. 111, 65–74.

Gerecke, A. C., Canonica, S., Müller, S. R., Schärer, M., Schwarzenbach, R. P., 2001. Quantification of dissolved natural organic matter (DOM) mediated phototransformation of phenylurea herbicides in lakes. Environ. Sci. Technol. 35, 3915–3923.

Girardi, C., Nowak, K. M., Carranza-Diaz, O., Lewkow, B., Miltner, A., Gehre, M., Schäffer, A., Kästner, M., 2013. Microbial degradation of the pharmaceutical ibuprofen and the herbicide 2,4-D in water and soil - Use and limits of data obtained from aqueous systems for predicting their fate in soil. Sci. Total Environ. 444, 32-42.

Glaeser, S. P., Berghoff, B. A., Stratmann, V., Grossart, H. P., Glaeser, J., 2014. Contrasting effects of singlet oxygen and hydrogen peroxide on bacterial community composition in a humic lake. PLoS One 9, e92518.

Groeneveld, M., Tranvik, L. J., Koehler, B., 2015. Photochemical mineralisation in a humic boreal lake - Temporal variability and contribution to carbon dioxide production. Biogeosciences Discuss. 12, 17125−17152.

Hāggmark, L., Ivarsson, K. I., Gollvik, S., Olofsson, P. O., 2000. Mesan, an operational mesoscale analysis system. Tellus A 52, 2−20.

Huang, J., Mabury, S. A., 2000. The role of carbonate radical in limiting the persistence of sulfur-containing chemicals in sunlit natural waters. Chemosphere 41, 1775–1782.

Kasten, F., Czeplak, G., 1980. Solar and terrestrial radiation dependent on the amount and type of cloud. Sol. Energy 24, 177–189.

Kellerman, A. M., Dittmar, T., Kothawala, D. M., Tranvik, L. J., 2014. Chemodiversity of dissolved organic matter in lakes driven by climate and hydrology. Nat. Commun. 5, 3804.

Koehler, B., Landelius, T., Weyhenmeyer, G. A., Machida, N., Tranvik, L. J., 2014. Sunlight-induced carbon dioxide emissions from inland waters. Glob. Biogeochem. Cycle 28, 696–711.

Koehler, B., Broman, E., Tranvik, L. J., 2016. Apparent quantum yield of photochemical dissolved organic carbon mineralization in lakes. Limnol. Oceanogr. 6, 2207-2221.

Larsen, S., Andersen, T. O. M., Hessen, D. O., 2011. Climate change predicted to cause severe increase of organic carbon in lakes. Glob. Change Biol. 17, 1186–1192.

Larson, R. A., Zepp, R. G., 1988. Reactivity of the carbonate radical with aniline derivatives. Environ. Toxicol. Chem. 7, 265–274.

Loiselle, S. A., Azza, N., Cozar, A., Bracchini, L., Tognazzi, A., Dattilo, A., Rossi, C., 2008. Variability in factors causing light attenuation in Lake Victoria. Freshwater Biol. 53, 535-545.

Matamoros, V., Duhec, A., Albaigés, J., Bayona, J. M., 2009. Photodegradation of carbamazepine, ibuprofen, ketoprofen and 17α-ethinylestradiol in fresh and seawater. Water Air Soil Pollut. 196, 161-168.

Mayer, B., Kylling, A., Emde, C., Hamann, U., Buras, R., 2011. libRadtran user's guide. http://www.libradtran.org/doc/libRadtran.pdf, last accessed June 2017.

Minella, M., Leoni, B., Salmaso, N., Savoye, L., Sommaruga, R., Vione, D., 2016. Long-term trends of chemical and modelled photochemical parameters in four Alpine lakes. Sci. Total Environ. 541, 247-256.

Monteith, D. T., Stoddard, J. L., Evans, C. D., De Wit, H. A., Forsius, M., Høgåsen, T., Wilander, A., Skjelkvåle, B. L., Jeffries, D. S., Vuorenmaa, J., 2007. Dissolved organic carbon trends resulting from changes in atmospheric deposition chemistry. Nature 450, 537–540.

Müller, R. A., Futter, M. N., Sobek, S., Nisell, J., Bishop, K., Weyhenmeyer, G. A., 2013. Water renewal along the aquatic continuum offsets cumulative retention by lakes: implications for the character of organic carbon in boreal lakes. Aquatic Sci. 75, 535-545.

Parker, K. M., Mitch, W. A., 2016. Halogen radicals contribute to photooxidation in coastal and estuarine waters. Proc. Natl. Acad. Sci. USA 113, 5868-5873.

Passananti, M., Temussi, F., Iesce, M. R., Previtera, L., Mailhot, G., Vione, D., Brigante, M., 2014. Photoenhanced transformation of nicotine in aquatic environments: Involvement of naturally occurring radical sources. Water Res. 55, 106–114.

Quintana, J. B., Weiss, S., Reemtsma, T., 2005. Pathways and metabolites of microbial degradation of selected acidic pharmaceutical and their occurrence in municipal wastewater treated by a membrane bioreactor. Water Res. 39, 2654-2664.

Quirós, R., 2003. The relationship between nitrate and ammonia concentrations in the pelagic zone of lakes. Limnetica 22, 37-50.

R. D. C. Team, 2014. R: A language and environment for statistical computing, edited. R Foundation for Statistical Computing, Vienna, Austria.

Richard, L. E., Peake, B. M., Rusak, S. A., Cooper, W. J., Burritt, D. J., 2007. Production and decomposition dynamics of hydrogen peroxide in freshwater. Environ. Chem. 4, 49-54.

Rosario-Ortiz, F. L., Canonica, S., 2016. Probe compounds to assess the photochemical activity of dissolved organic matter. Environ. Sci. Technol. 50, 12532-12547.

Sobek, S., Tranvik, L. J., Prairie, Y. T., Kortelainen, P., Cole, J. J., 2007. Patterns and regulation of dissolved organic carbon: An analysis of 7,500 widely distributed lakes. Limnol. Oceanogr. *58*, 1208–1219.

Stubbins, A., Spencer, R. G. M., Chen, H., Hatcher, P. G., Mopper, K., Hernes, P. J., Mwamba, V. L., Manganu, A. M., Wabakanghanzi, J. N., Six, J., 2010. Illuminated darkness: Molecular signatures of Congo River dissolved organic matter and its photochemical alteration as revealed by ultrahigh resolution mass spectrometry. Limnol. Oceanogr. 55, 1467-1477.

Verpoorter, C., Kutser, T., Seekell, D. A., Tranvik, L. J., 2014. A global inventory of lakes based on high-resolution satellite imagery. Geophys. Res. Lett. 41, 6396–6402.

Vione, D., Khanra, S., Cucu Man, S., Maddigapu, P. R., Das, R., Arsene, C., Olariu, R. I., Maurino, V., Minero, C., 2009. Inhibition vs. enhancement of the nitrate-induced phototransformation of organic substrates by the $^{\bullet}OH$ scavengers bicarbonate and carbonate. Water Res. 43, 4718 – 4728.

Vione, D., Maddigapu, P. R., De Laurentiis, E., Minella, M., Pazzi, M., Maurino, V., Minero, C., Kouras, S., Richard, C., 2011. Modelling the photochemical fate of ibuprofen in surface waters. Water Res. 45, 6725−6736.

Vione, D., Minella, M., Maurino, V., Minero, C., 2014. Indirect photochemistry in sunlit surface waters: Photoinduced production of reactive transient species. Chem.-Eur. J. 20, 10590−10606.

Vione, D., Calza, P., Galli, F., Fabbri, D., Santoro, V., Medana, C., 2015. The role of direct photolysis and indirect photochemistry in the environmental fate of ethylhexyl methoxy cinnamate (EHMC) in surface waters. Sci. Total Environ. 537, 58−68

Wallace, D. F., Hand, L. H., Oliver, R. G., 2010. The role of indirect photolysis in limiting the persistence of crop protection products in surface waters. Environ. Toxicol. Chem. 29, 575–581.

Wenk, J., Von Gunten, U., Canonica, S., 2011. Effect of dissolved organic matter on the transformation of contaminants induced by excited triplet states and the hydroxyl radical. Environ. Sci. Technol. 45, 1334–1340.

Wols, B., Hofman-Caris, C., 2012. Review of photochemical reaction constants of organic micropollutants required for UV advanced oxidation processes in water. Water Res. 46, 2815−2827.

Yan, S., Song, W., 2014. Photo-transformation of pharmaceutically active compounds in the aqueous environment: a review. Environ. Sci.-Process Impacts 16, 697–720.

Zou, H., Radke, M., Kierkegaard, A., McLachlan, M. S., 2015a. Temporal Variation of Chemical Persistence in a Swedish Lake Assessed by Benchmarking. Environ. Sci. Technol. 49, 9881–9888.

Zou, H., Radke, M., Kierkegaard, A., MacLeod, M., McLachlan, M. S., 2015b. Using chemical benchmarking to determine the persistence of chemicals in a Swedish lake. Environ. Sci. Technol. 49, 1646–1653.

Table 1. Direct photolysis quantum yields (Φ_S) and second-order reaction rate constants ($k_{S,J}$) with the main photoinduced transients (J = $^{\bullet}OH$, $^3CDOM^*$, $^1O_2$ or $CO_3^{-\bullet}$) of the example compounds used for photochemical modeling, with S = acetaminophen (APAP), dimethomorph (DMM), ethylhexyl methoxycinnamate (EHMC), fenuron (FEN), and nicotine (NIC) (Avetta et al., 2014; De Laurentiis et al., 2014; Passananti et al., 2014; Fabbri et al., 2015; Vione et al., 2015). n/a = not available.

	APAP	**DMM**	**EHMC**	**FEN**	**NIC**
Φ_S (unitless)	$4.6\cdot10^{-2}$	$2.6\cdot10^{-5}$	$3.8\cdot10^{-2}$	$6\cdot10^{-3}$	n/a
$k_{S,^{\bullet}OH}$ (L mol^{-1} s^{-1})	$1.9\cdot10^{9}$	$2.6\cdot10^{10}$	$1\cdot10^{10}$	$7\cdot10^{9}$	$1.1\cdot10^{9}$
$k_{S,^3CDOM*}$ (L mol^{-1} s^{-1})	$1.1\cdot10^{10}$	$1.6\cdot10^{9}$	$5\cdot10^{9}$	$2\cdot10^{9}$	n/a
$k_{S,^1O_2}$ (L mol^{-1} s^{-1})	$3.7\cdot10^{7}$	$8.5\cdot10^{5}$	$1.5\cdot10^{7}$	$< 1\cdot10^{6}$	$3.4\cdot10^{6}$
$k_{S,CO_3^{-\bullet}}$ (L mol^{-1} s^{-1})	$3.8\cdot10^{8}$	$< 1\cdot10^{6}$	$< 1\cdot10^{6}$	$6\cdot10^{6}$	$< 1\cdot10^{6}$

Table 2. Example compounds used to assess the photoreaction kinetics. For each compound, the main reaction pathways involved in phototransformation in temperate lakes are listed. Earlier reported photochemical half-life times in temperate lakes are included, for comparison with the half-life times obtained in this study for boreal lakes. The right column reports some compounds and compound classes that are expected to also undergo important phototransformation via the most important reaction pathway(s) highlighted in the previous column (Buxton et al., 1988; Huang and Mabury, 2000; Gerecke et al., 2001; Richard et al., 2007; Wenk et al., 2011; Avetta et al., 2014; De Laurentiis et al., 2014; Yan and Song, 2014). SE = standard error.

Sample compound	**Major photoreaction pathway in temperate lakes, with minor photoreaction pathways in brackets**	**Photochemical half-life time in temperate lakes (days; see refs. in the table caption)**	**Mean (±SE) photochemical half-life time in boreal lakes (days; this study)**	**Relevance of the major photoreaction pathway for broader classes of dissolved compounds (compounds main uses are reported in brackets)**
Acetaminophen (APAP)	$CO_3^{-\bullet}$, (^{3}CDOM*, direct photolysis)	5-14	15.0±0.5	$CO_3^{-\bullet}$: Aromatic amines, thiols (pesticides, pharmaceuticals, dyes and odors)
Fenuron (FEN)	^{3}CDOM*, ($^\bullet$OH)	10-50	73±2	^{3}CDOM*: Phenylurea herbicides, phenols, (plastic, medical drugs

				and herbicides)
Nicotine (NIC)	$^{\bullet}OH$, ($^{1}O_2$)	50-300	5200±100	$^{\bullet}OH$: Toluene (industrial feedstock and solvent), carbamazepine (medical drug)
Ethylhexyl methoxycinnamate (EHMC)	Direct photolysis	<2	12.0 ± 0.3	Direct photolysis: Solar filters, triclosan (antibacterial and antifungal agent), some cephalosporin antibiotics, nitrobenzene (precursor to rubber chemicals, pesticides, dyes, explosives and pharmaceuticals)
Dimethomorph (DMM)	^{3}CDOM* and $^{\bullet}OH$ (direct photolysis)	10-40	70.7 ± 1.3	^{3}CDOM*: Phenols, phenylurea herbicides. $^{\bullet}OH$: Toluene, carbamazepine

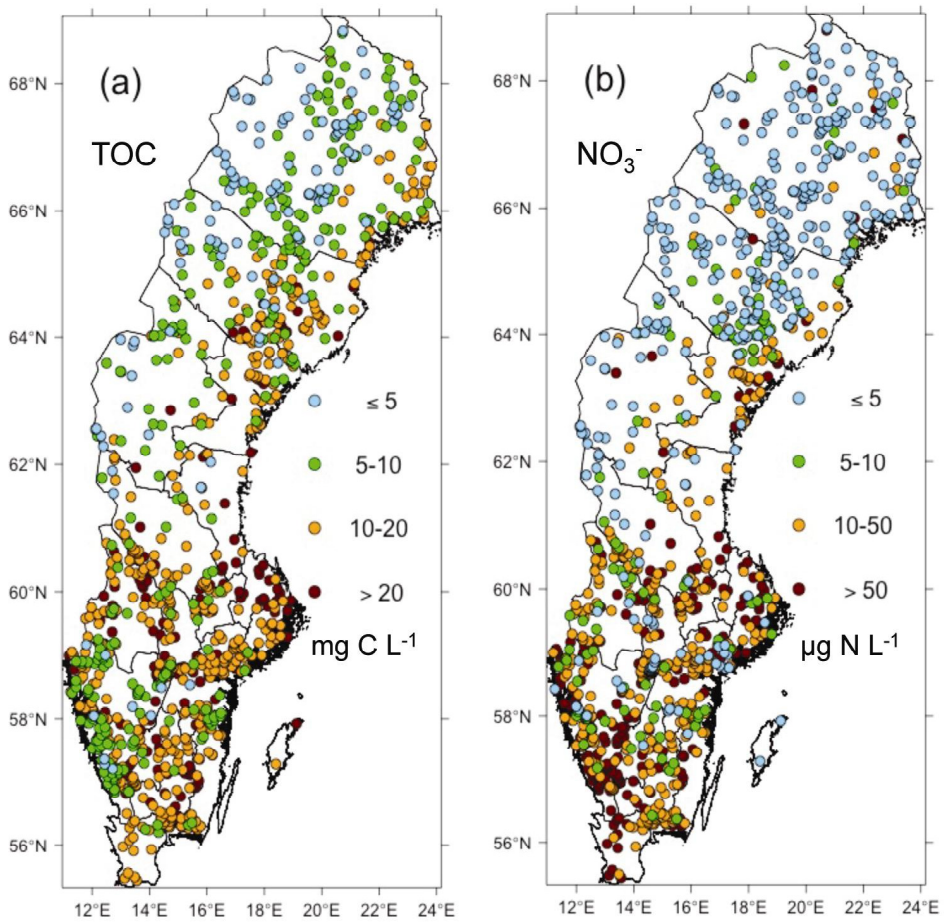

Figure 1. Map of Sweden showing the location of the 1048 modeling study lakes (circles), color-coded according to concentrations of TOC (a, $mg_C\ L^{-1}$) and nitrate (b, $\mu g_N\ L^{-1}$). The color coding of the classes are given in each panel, and the lines denote the counties of Sweden.

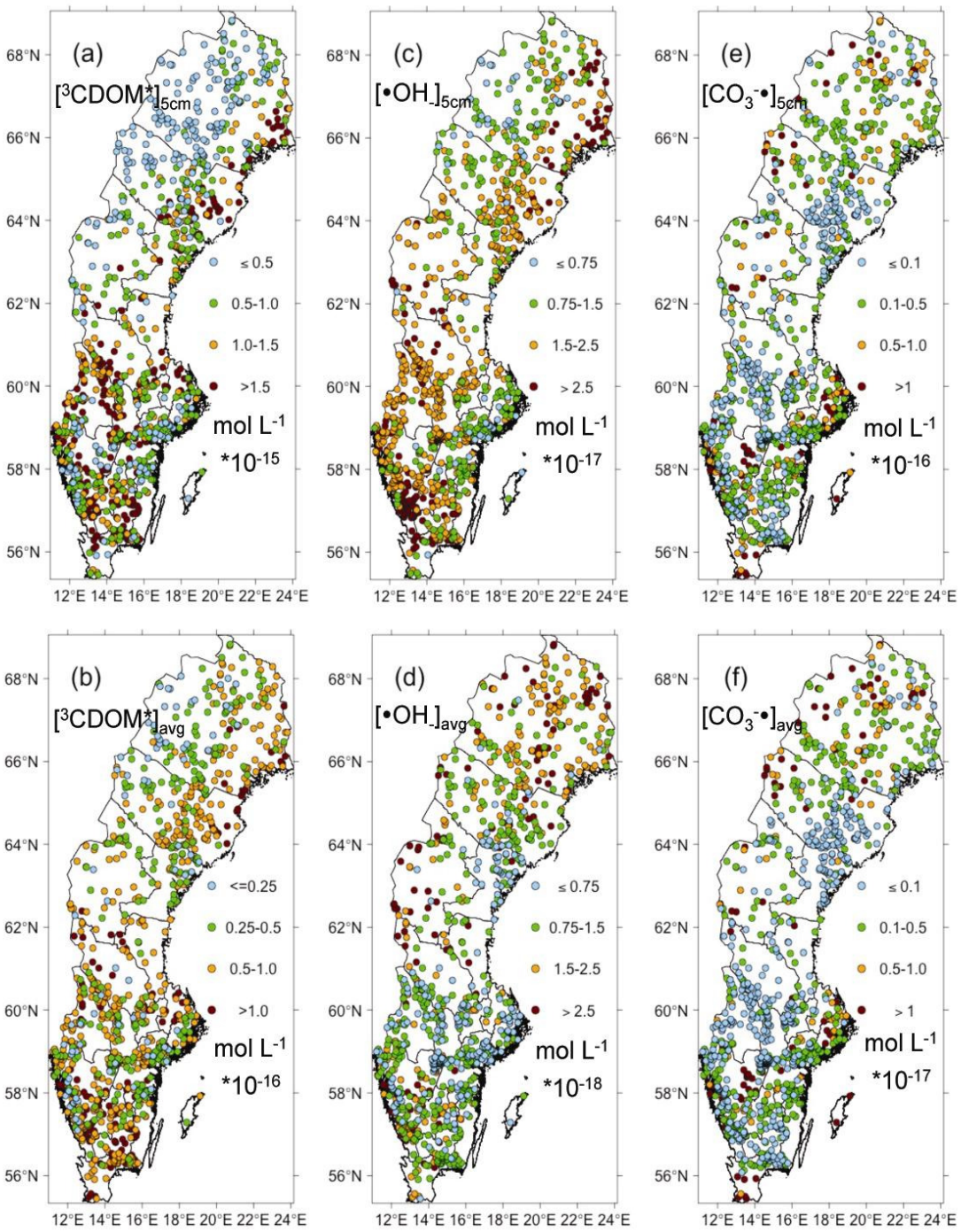

Figure 2. The location of the 1048 modeling study lakes (circles) across Sweden, color-coded according to simulated day-averaged steady state concentrations of the reactive transients: (a,b) CDOM triplet states (^{3}CDOM*), (c,d) hydroxyl radicals ($^\bullet$OH) and (e,f) carbonate radical anions ($CO_3^{-\bullet}$). The upper (a,c,e) and lower (b,d,f) rows show mean concentrations down to 0.05 m and down to the average depth of each lake, respectively. The color coding of the classes are given in each panel, and the concentrations are expressed in mol L^{-1} times 10^{-15} (a), 10^{-16} (b,e), 10^{-17} (c,f) and 10^{-18} (d). The lines denote the counties of Sweden.

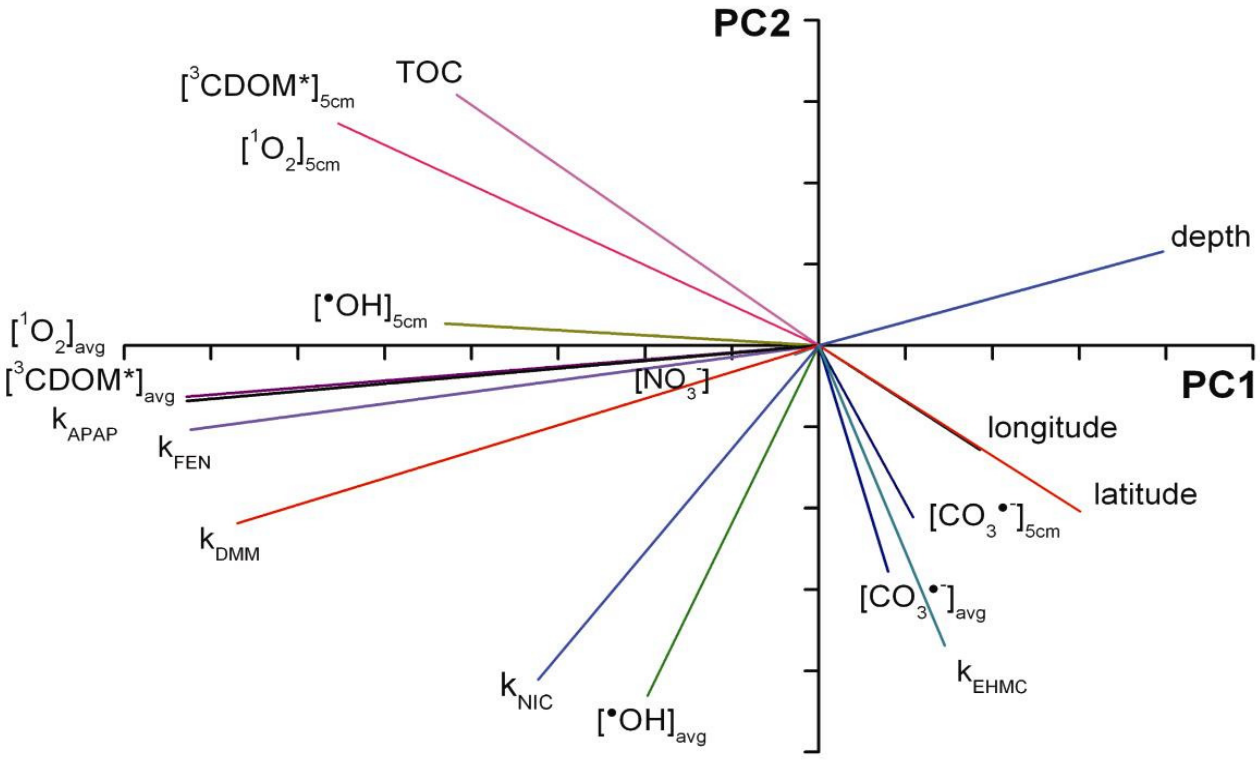

Figure 3. The loadings that resulted from the Principal Components Analysis (PCA) on the whole dataset. The percent explained variance on the first and second principal component was 38.9 and 23.2%, respectively. k_{FEN}, k_{EHMC}, k_{DMM}, k_{NIC} and k_{APAP} are the pseudo first order kinetic constants for the photochemical degradation of fenuron (FEN), ethylhexyl methoxycinnamate (EHMC), dimethomorph (DMM), nicotine (NIC) and acetaminophen (APAP), respectively. They are related to the half-life times $t_{½}$ by the relationship $k = \ln 2\ (t_{½})^{-1}$. $[J]_{avg}$ and $[J]_{5cm}$ are the concentrations of the photochemically generated J transients ($^{\bullet}OH$, $CO_3^{-\bullet}$, $^3CDOM^*$ and $^1O_2$) averaged down to the mean depth of each lake and in the first 0.05 m of water, respectively.

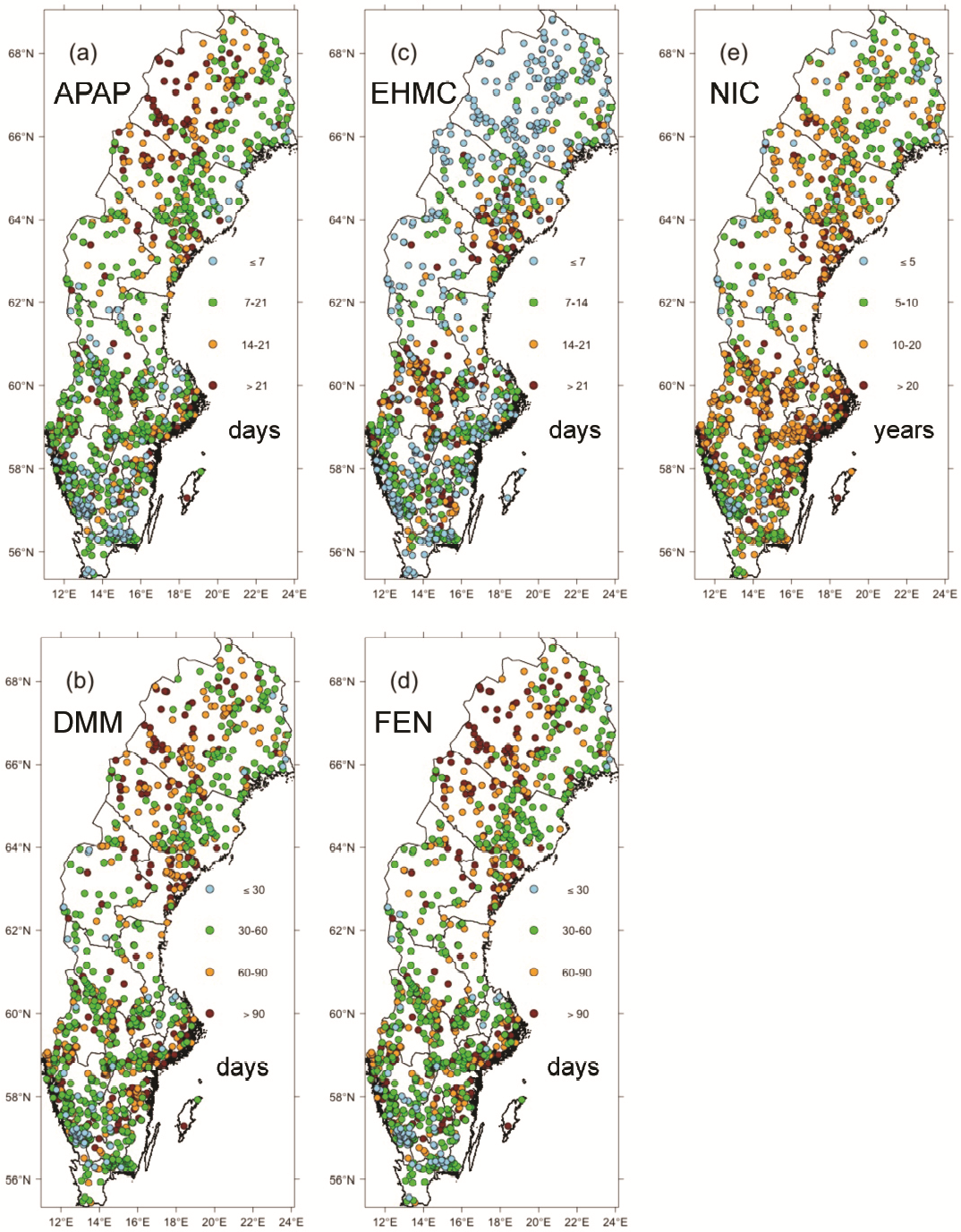

Figure 4. Map of Sweden showing the location of the 1048 modeling study lakes (circles), colour-coded according to the simulated half-life times of five organic pollutants: (a) acetaminophen (APAP); (b) dimethomorph (DMM); (c) ethylhexyl methoxycinnamate (EHMC); (d) fenuron (FEN), and (e) nicotine (NIC). The colour coding of the classes are given in each panel, and the lifetimes are expressed in days (a-d) or years (e). The lines denote the counties of Sweden.

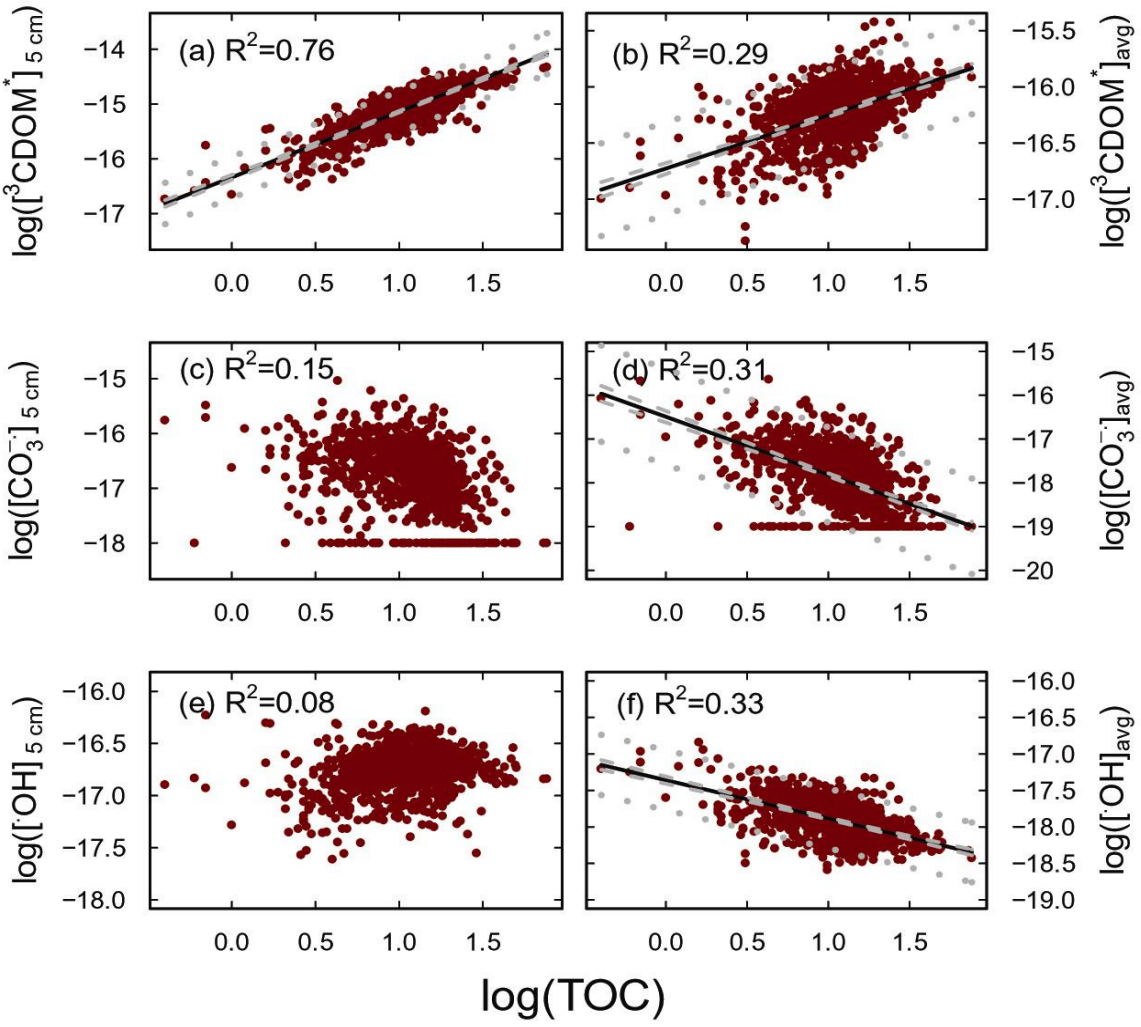

Figure 5. Scatterplots between the logarithmically transformed steady-state concentrations of the simulated photoreactive transients (mol L^{-1}) and the logarithmically transformed total organic carbon concentration (TOC, mg_C L^{-1}), down to 0.05 m lake water depth for (a) ^{3}CDOM*, (c) $CO_3^{-\bullet}$ and (e) $^\bullet$OH, and down to the average depth of each lake for (b) ^{3}CDOM*, (d) $CO_3^{-\bullet}$ and (f) $^\bullet$OH. When R^2 exceeded 0.25 (i.e. in (a), (b), (d) and (f)), linear regression lines are included (solid black) with 95% confidence intervals (dashed gray) and 95% prediction intervals (dotted gray). The *P*-value was smaller than 0.05 for the other relationships as well but given the small amount of explained variability (R^2) we did not consider these. The dataset of $CO_3^{-\bullet}$ concentrations included 116 zero values, for the lakes with zero or negative alkalinity. In these cases, a small positive constant value was added to the dataset before log-transformation (10^{-18} in (c) and 10^{-19} in (d)). Plots with $^1O_2$ (Fig. SM3) are not shown here because they are very similar to those with ^{3}CDOM*.